# Tunnel magnetoresistance and spin torque switching in MgO-based magnetic tunnel junctions with a Co/Ni multilayer electrode

Takahiro Moriyama,[a] Theodore J. Gudmundsen, Pinshane Y. Huang, Luqiao Liu, David A. Muller, Daniel C. Ralph, and Robert A. Buhrman
*Cornell University, Ithaca, New York 14853, USA*

(Received 5 April 2010; accepted 1 August 2010; published online 20 August 2010)

We have fabricated MgO-barrier magnetic tunnel junctions with a Co/Ni switching layer to reduce the demagnetizing field via interface anisotropy. With a fcc-(111) oriented Co/Ni multilayer combined with an FeCoB insertion layer, the demagnetizing field is 2 kOe and the tunnel magnetoresistance can be as high as 106%. Room-temperature measurements of spin-torque switching are in good agreement with predictions for a reduced critical current associated with the small demagnetization for antiparallel-to-parallel switching. For parallel-to-antiparallel switching the small demagnetization field causes spatially nonuniform reversal nucleated at the sample ends, with a low energy barrier but a higher switching current. © *2010 American Institute of Physics*. [doi:10.1063/1.3481798]

MgO-based magnetic tunnel junctions (MTJs) with a large tunneling magnetoresistance (TMR) (Refs. 1–4) whose magnetic orientations can be controlled by spin-torque switching[5–7] are promising candidates for magnetic random access memories.[8] However, for widespread application it will be necessary to reduce the switching current density while maintaining thermal stability for the magnetic states. One strategy is to employ a magnetic switching layer with large perpendicular magnetic anisotropy, such that the equilibrium magnetization direction is perpendicular to the sample plane.[9–11] Here we investigate an alternative strategy of tuning the perpendicular anisotropy of the switching layer to reduce the demagnetization field but to keep the equilibrium orientation of the switching layer in the sample plane. We show that low-demagnetization fcc-(111)-oriented Co/Ni multilayers can be integrated with MgO tunnel junctions to give high TMR, and that the low demagnetization field of the Co/Ni can provide significant reduction in the spin-torque switching current.

For an in-plane magnetized switching layer within a macrospin approximation for the magnetization dynamics, the critical current for spin-torque switching for an MTJ in the absence of thermal fluctuations has the approximate form[7,12–14]

$$I_{c0} \approx \frac{2e}{\hbar}\frac{\alpha M_s V}{\eta(\theta)}\left(H_{c0}+\frac{H_{\mathrm{eff}}}{2}\right), \tag{1}$$

where $\alpha$ is the damping constant, $M_s$ is the saturation magnetization of the switching layer, $V$ is the volume of the layer, $\eta(\theta)=p/(1+p^2)$ for parallel-to-antiparallel (P-to-AP) switching and $\eta(\theta)=p/(1-p^2)$ for AP-to-P switching where the spin polarization $p=\sqrt{\mathrm{TMR}/(\mathrm{TMR}+2)}$,[13,14] $H_{c0}$ is the coercive field in the absence of thermal fluctuations, and $H_{\mathrm{eff}}$ is the effective demagnetizing field. For a uniform transition-metal magnetic film, $H_{\mathrm{eff}}$ is generally determined by the saturation magnetization, $H_{\mathrm{eff}}\approx 4\pi M_S \approx 10$ kOe, while $H_{c0}$ is much smaller, usually $\approx$100 Oe as determined by lateral shape anisotropy. However, the thermal stability of the magnetic bit is governed by $H_{c0}$, and does not depend on $H_{\mathrm{eff}}$ as long as $H_{c0}<H_{\mathrm{eff}}$. This suggests that $I_{c0}$ may be reduced by using the interface anisotropy of multilayers like Co/Ni to decrease $H_{\mathrm{eff}}$,[15] while leaving $H_{c0}$ unchanged so as to maintain thermal stability. In previous work, employing a Co/Ni multilayer within all-metal spin valves,[16] our group demonstrated a factor of 5 reduction in $I_{c0}$ relative to control samples, but all-metal spin valves lack the large TMR provided by MgO-based MTJs that is necessary for applications. Incorporating a Co/Ni electrode with an MgO tunnel barrier is nontrivial, since multilayer Co/Ni has an fcc-(111) structure that does not provide the same band matching to MgO(001) employed in high-TMR MTJs with bcc-(001) Fe or FeCoB electrodes.[1–4] We report the fabrication of high-TMR MTJs with reduced-demagnetization switching layers consisting of a Co/Ni multilayer together with a thin FeCoB insertion layer contacting the MgO. We characterize the crystal structure of the interface and discuss the TMR and spin-transfer switching characteristics of these junctions.

Our MTJ layer stack was prepared on $SiO_2$/Si(001) wafers by a magnetron sputtering with a base pressure of $10^{-9}$ Torr. The layer structure is Ta(3)/$[$CuN(20)/Ta(3)$]_2$/Cu(2) / $[$Co(0.4) / Ni(0.8)$]_2$ / $Fe_{60}Co_{20}B_{20}$(1.1) / MgO(t) / $Fe_{60}Co_{20}B_{20}$(20)/Ta(8)/Pt(30). The numbers in the parentheses are the layer thicknesses in nanometers. The MgO is formed by rf magnetron sputtering with an oxygen getter driven by sputtered tantalum. The MgO thickness, $t$, was varied from 0.7 to 1.5 nm across the wafer. After the deposition of all layers, the wafers were annealed in a $N_2$ atmosphere at 375 °C for up to 10 min on a sample stage allowing a fast cooling rate of 43 °C/min. Individual tunnel junctions were then patterned using electron-beam lithography and ion-beam etching. X-ray diffraction measurements (not shown) indicate the $[$Co(0.4)/Ni(0.8)$]_2$ layer is (111)-textured, as is required for interface anisotropy in Co/Ni multilayers. The 1.1 nm FeCoB layer is designed to provide a buffer for a lattice matching between fcc-CoNi(111) and MgO(001) while reducing only slightly the mean perpendicular anisotropy. Magnetization measurements show that the equilibrium moment of the $[$Co(0.4)/Ni(0.8)$]_2$/FeCoB(1.1) film lies in plane with a perpendicular

[a]Electronic mail: tm376@cornell.edu.

 

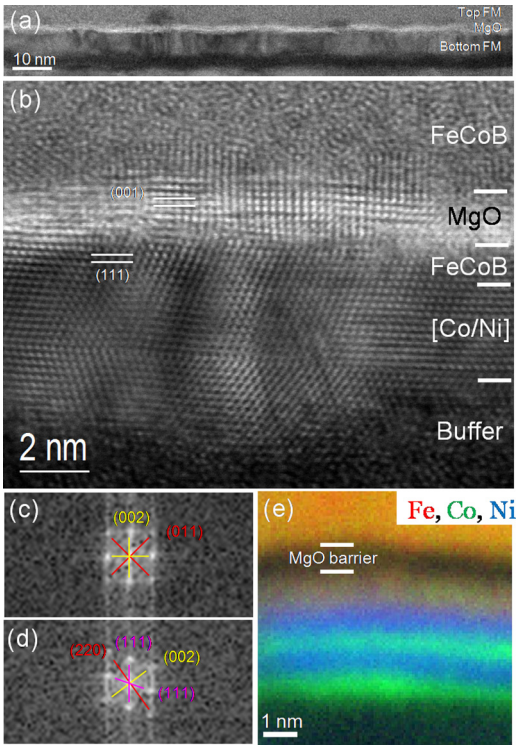


FIG. 1. (Color online) [(a) and (b)] Bright-field STEM images of an MTJ with the $[Co/Ni]_2/FeCoB$ electrode. (c) Fourier-transformed image of the MgO region and (d) the FeCoB insertion layer. (e) EELS image with colors indicating the concentrations of Fe, Co, and Ni.

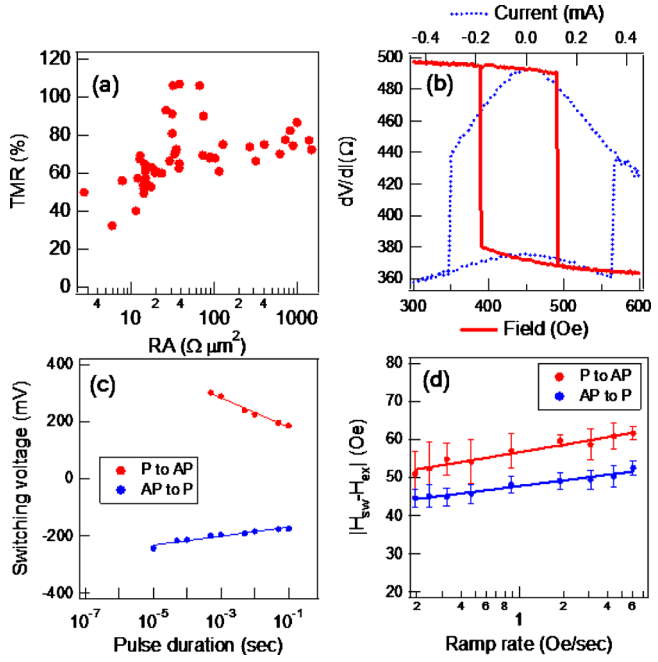


FIG. 2. (Color online) (a) Dependence of TMR on the resistance-area product. (b) Room temperature differential resistance showing magnetic-field-driven switching and spin-torque driven switching for a device (lateral size: $70\times220$ nm$^2$) with 38% TMR. [(c) and (d)] Analysis of switching voltages as a function of (c) pulse duration and (d) magnetic-field ramp rate for the same device as in (b). For the current-switching measurements in (b) and (d), an external field $H=460$ Oe was applied to counteract the average dipole field from the fixed layer.

saturation field of 2 kOe, which indicates that the demagnetizing field is reduced by about 10 kOe relative to the averaged saturation magnetization of 12 kOe. From ferromagnetic resonance measurements, the Gilbert damping parameter of the $[Co(0.4)/Ni(0.8)]_2/FeCoB(1.1)$ film is $\alpha=0.015\pm0.005$.

Figure 1 shows scanning transmission electron microscopy (STEM) images and electron energy loss spectroscopy (EELS) composition maps[17] of the MTJ layer stack after a 3 min anneal, for which we achieved room-temperature TMR ratios as large as 106% [see Fig. 2(a)]. We observe a high degree of crystal coherence extending from the Co/Ni multilayer up through the FeCoB insertion layer to the MgO [Fig. 1(b)]. The crystal lattice at the lower FeCoB/MgO interface seems to be partially matched by introducing dislocations. The fcc-$(\bar{1}10)$ face of the Co/Ni multilayer and (100) face of the MgO are oriented together in the plane of the STEM image [Fig. 1(b)]. From the Fourier transform of the MgO lattice image [Fig. 1(c)], the tunnel barrier has the usual cubic structure with only a compression by 3% in [001] direction. The Fourier transform of the image of the lower FeCoB region [Fig. 1(d)] indicates that the FeCoB insertion layer is crystallized in a strained fcc structure rather than the usual bcc, and has the same orientation as the Co/Ni multilayer. We therefore conclude that the structure at the lower interface of the tunnel barrier is fcc-FeCoB(111)[$\bar{1}$10]/MgO(001)[100] rather than the bcc-FeCoB(001)[110]/MgO(001)[100] structure ordinarily used for high-TMR junctions. The upper FeCoB layer is crystallized only near the interface with MgO, in the usual bcc-FeCoB(001)[110]/MgO(001)[100] relationship, most likely due to its greater thickness. This could be reduced by using an antiferromagnetic pinning layer. The EELS image [Fig. 1(e)] shows that the $[Co/Ni]_2/FeCoB$ film maintains its layer structure without large-scale intermixing. EELS also reveals that the annealed barrier is Mg(B)O.[18]

The switching properties of a $70\times220$ nm$^2$ device with $RA=4.3$ Ω μm$^2$ and TMR=38% are shown in Fig. 2(b). The minor loop as a function of in-plane magnetic field indicates an ~52 Oe coercive field and an average dipole field from the fixed layer of 460 Oe. The hysteresis loop for spin-torque switching as a function of current, for an applied field that cancels the average dipole field, shows quasistatic room-temperature switching currents for AP-to-P and P-to-AP switching of −0.31 mA and 0.35 mA, respectively. To estimate the effective activation energy $E_a$ and the zero-thermal-fluctuation critical current $I_{c0}$, we performed both current-pulse [Fig. 2(c)] and field-ramp measurements [Fig. 2(d)]. Assuming that current-induced heating effects are negligible, for thermally activated switching the average switching current $\langle I_c\rangle$ and the switching field $\langle H_c\rangle$ measured relative to 460 Oe should take the forms[19,20]

$$\langle I_c\rangle = I_{c0}\left[1-\frac{k_BT}{E_a}\ln(t_p/\tau_0)\right], \tag{2}$$

$$\langle H_c\rangle = H_{c0}(T)\left\{1-\left[\frac{k_BT}{E_a}\ln\left(\frac{1}{\tau_0|R_H|\ln 2}\right)\right]^{2/3}\right\}, \tag{3}$$

where $k_B$ is Boltzmann's constant, $t_p$ is the pulse duration, $R_H$ is the ramp rate for field, and $\tau_0$ is the inverse of the attempt frequency which we assume to be $10^{-9}$ s. From the fits to the current-pulse data in Fig. 2(c), we obtain for AP-to-P switching $E_{a,\text{AP-P}}=1.12\pm0.07$ eV and $I_{c0,\text{AP-P}}=0.60\pm0.02$ mA (corresponding to $5.0\times10^6$ A/cm$^2$) and for P-to-AP switch-

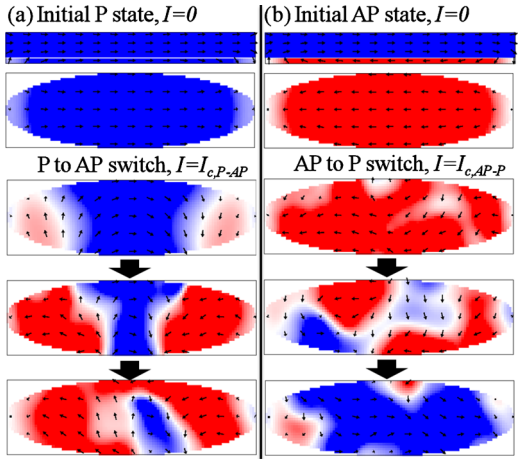


FIG. 3. (Color online) Results of zero-temperature micromagnetic simulations for the magnetization dynamics of the switching layer during (a) P-to-AP and (b) AP-to-P current-driven switching. In both cases an external field is applied to cancel the average dipole field from the fixed layer. The color gradation indicates the in-plane horizontal component of the magnetization. The top two panels in both (a) and (b) show the initial static state for zero current in side and top views. The bottom three panels show the time evolution of the switching layer: just after the application of the current pulse, at the midpoint of the switching transition, and at 80% of full reversal.

ing $E_{a,\text{P-AP}}=0.68\pm0.02$ eV and $I_{c0,\text{P-AP}}=1.60\pm0.06$ mA ($1.3\times10^7$ A/cm$^2$). From the fits to the field-ramp data in Fig. 2(d), we obtain for AP-to-P switching $E_{a,\text{AP-P}}=1.22\pm0.06$ eV and $H_{c0,\text{AP-P}}=115\pm5$ Oe and for P-to-AP switching $E_{a,\text{P-AP}}=1.14\pm0.06$ eV and $H_{c0,\text{P-AP}}=146\pm8$ Oe. The five other devices studied gave similar results.

We can compare the results for the zero temperature switching currents to the values expected from Eq. (1). Using $\alpha=0.015$, $4\pi M_s=12$ kOe, $H_{c0}=130$ Oe, $H_{\text{eff}}=2$ kOe, and $p=0.4$ based on the TMR=38%, Eq. (1) predicts $I_{c0,\text{AP-P}}=0.61$ mA ($5.0\times10^6$ A/cm$^2$) and $I_{c0,\text{P-AP}}\approx0.44$ mA ($3.7\times10^6$ A/cm$^2$). Our measured critical current for AP-to-P switching is in good agreement with the predicted value, confirming that the reduction in the demagnetization field from 12 to 2 kOe has the desired effect of reducing $I_{c0}$. The extrapolated zero-temperature switching current for P-to-AP switching, 1.60 mA, is however larger than expected from theory, and this value is associated with an activation energy much smaller than for current-induced AP-to-P switching or for either direction of field-induced switching. We have performed zero-temperature micromagnetic simulations [using OOMMF (Ref. 21) modified with the Slonczewski spin torque term] to try to understand this difference. The simulations shown in Fig. 3 predict that in equilibrium the magnetization of the switching layer has significant curling that causes the moments near the sample ends to be oriented almost perpendicular to the sample plane, due to the small demagnetizing field, the dipole field from the fixed layer, and the relatively large sample size. For current-driven P-to-AP switching, this edge curling leads to a strongly spatially nonuniform reversal mode that is nucleated near the sample ends and propagates to the interior. This switching mode may explain the low activation energy and large extrapolated critical current that we observe. For current-driven AP-to-P switching, the simulations suggest (despite the presence of the edge curling) that reversal is initiated in the interior of the sample, away from the ends.

In summary, we have fabricated MgO-based MTJs with a Co/Ni switching layer having a reduced demagnetizing field. Although the structure of this layer is fcc-(111) rather than bcc-(001) as required for optimum band matching to MgO, we nevertheless obtain TMR values as large as 106%. For AP-to-P spin-torque switching we determine a zero-thermal-fluctuation critical current density of $5.0\times10^6$ A/cm$^2$, in agreement with predictions for the effect of the reduced demagnetization field. For P-to-AP switching, the critical current density is higher, which simulations suggest is due to a spatially nonuniform, edge-dominated reversal mode made more favorable by the small demagnetization field. In future work, the dipole field from the pinned layer can be decreased through use of a pinned synthetic antiferromagnetic layer to inhibit the nonuniform mode, and the switching currents may be further reduced by using switching layers with smaller total magnetic moments and higher tunneling polarizations.

We thank John Read (NIST) for performing FMR on our film stacks. This work was supported by NSF/NSEC through the Cornell Center for Nanoscale Systems, NSF/IGERT, ONR, and ARO (Grant Nos. DGE-0654193, N00014-06-1-0428, and W911NF-08-2-0032). We also acknowledge NSF support through use of the Cornell Nanofabrication Facility/NNIN and the Cornell Center for Materials Research facilities.

[1] J. Mathon and A. Umerski, Phys. Rev. B **63**, 220403 (2001).
[2] W. H. Butler, X. G. Zhang, T. C. Schulthess, and J. M. MacLaren, Phys. Rev. B **63**, 054416 (2001).
[3] S. S. P. Parkin, C. Kaiser, A. Panchula, P. M. Rice, B. Hughes, M. Samant, and S. H. Yang, Nature Mater. **3**, 862 (2004).
[4] S. Yuasa, T. Nagahama, A. Fukushima, Y. Suzuki, and K. Ando, Nature Mater. **3**, 868 (2004).
[5] J. C. Slonczewski, J. Magn. Magn. Mater. **159**, L1 (1996).
[6] L. Berger, Phys. Rev. B **54**, 9353 (1996).
[7] D. C. Ralph and M. D. Stiles, J. Magn. Magn. Mater. **320**, 1190 (2008).
[8] J. A. Katine and E. E. Fullerton, J. Magn. Magn. Mater. **320**, 1217 (2008).
[9] S. Mangin, D. Ravelosona, J. A. Katine, M. J. Carey, B. D. Terris, and E. E. Fullerton, Nature Mater. **5**, 210 (2006).
[10] S. Mangin, Y. Henry, D. Ravelosona, J. A. Katine, and E. E. Fullerton, Appl. Phys. Lett. **94**, 012502 (2009).
[11] M. Yoshikawa, E. Kitagawa, T. Nagase, T. Daibou, M. Nagamine, K. Nishiyama, T. Kishi, and H. Yoda, IEEE Trans. Magn. **44**, 2573 (2008).
[12] J. Z. Sun, Phys. Rev. B **62**, 570 (2000).
[13] J. C. Slonczewski and J. Z. Sun, J. Magn. Magn. Mater. **310**, 169 (2007).
[14] J. Z. Sun and D. C. Ralph, J. Magn. Magn. Mater. **320**, 1227 (2008).
[15] G. H. O. Daalderop, P. J. Kelly, and F. J. A. Denbroeder, Phys. Rev. Lett. **68**, 682 (1992).
[16] L. Q. Liu, T. Moriyama, D. C. Ralph, and R. A. Buhrman, Appl. Phys. Lett. **94**, 122508 (2009).
[17] D. A. Muller, L. F. Kourkoutis, M. Murfitt, J. H. Song, H. Y. Hwang, J. Silcox, N. Delby, and O. L. Krivanek, Science **319**, 1073 (2008).
[18] J. C. Read, J. J. Cha, W. F. Egelhoff, H. W. Tseng, P. Y. Huang, Y. Li, D. A. Muller, and R. A. Buhrman, Appl. Phys. Lett. **94**, 112504 (2009).
[19] J. Kurkijärvi, Phys. Rev. B **6**, 832 (1972).
[20] M. P. Sharrock, IEEE Trans. Magn. **26**, 193 (1990).
[21] M. J. Donahue and D. G. Porter, OOMMF User's Guide, Version 1.0, National Institute of Standards and Technology, Technical Report No. NISTIR 6376, 1999.